Modeling of a regenerative indirect evaporative cooler for a desiccant cooling system

Bellemo, Lorenzo; Elmegaard, Brian; Reinholdt, Lars O. ; Kærn, Martin Ryhl

Publication date:
2013

MODELING OF A REGENERATIVE INDIRECT EVAPORATIVE COOLER FOR A DESICCANT COOLING SYSTEM

Lorenzo Bellemo[(a)], Brian Elmegaard[(a)], Lars O. Reinholdt [(b)], Martin R. Kærn[(a)]

[(a)] Technical University of Denmark, Department of Mechanical Engineering, Section of Thermal Energy, 2800 Kongens Lyngby, Denmark, lobel@mek.dtu.dk
[(b)] Danish Technological Institute, Energy and Climate Division, Refrigeration and Heat Pump Technology, 8000 Aarhus, Denmark

ABSTRACT

This paper presents a numerical study of a regenerative indirect evaporative cooler, the so-called Dew Point Cooler (DPC), which is part of a Desiccant Cooling system that may both dehumidify and cool humid air. The DPC model is based on first principles using a 1D finite volume scheme and determines the steady state working conditions for the component. A sensitivity analysis of the DPC performance is carried out based on the air inlet conditions, air flow rate and recirculation fraction. A recirculation fraction around 0.3 maximizes the DPC net cooling capacity. The supply temperature is found to be mostly affected by the inlet humidity ratio. Manufacturer data are used to tune the model. The tuned DPC model is characterized by an area effectiveness coefficient which is kept constant at 0.55. The cooling capacity and water consumption estimated by the tuned model deviate within 3% and 8%, respectively from manufacturer data. The computed pressure drops deviates within 6% from manufacturer data.

1. INTRODUCTION

Desiccant Cooling (DEC) systems are thermally driven air conditioning systems. Compared to vapor compression cycle (VCC) based systems, DEC systems can reduce electricity consumption and environmental impact, particularly when the need for dehumidification increases, Daou et al. (2006). DEC systems use a desiccant dehumidifier to decrease the moisture content of a process airstream, which is then cooled by a cooling unit. An additional heat recovery unit between the desiccant dehumidifier and the cooling unit may be needed to precool the process airstream. Therefore, DEC systems are able to decouple latent load and sensible load, which is different from VCC-based systems. Desiccant dehumidifiers dry and heat the process airstream simultaneously until the desiccant is saturated; at this point moisture has to be rejected from the desiccant to provide a continuous dehumidification. Moisture rejection, also called regeneration, is achieved by heating the desiccant up to a sufficiently high temperature. Heat is provided by a thermal source connected to the desiccant dehumidifier. Fig. 1 shows a general scheme of the described structure of DEC systems.

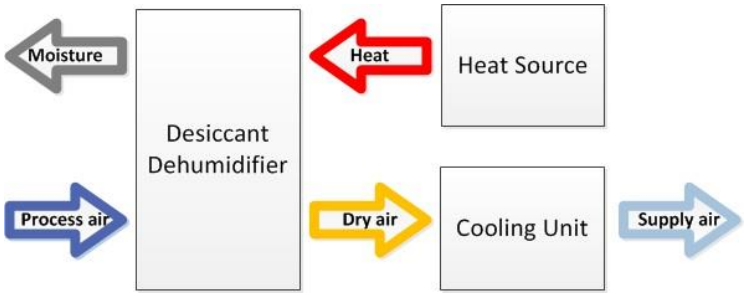

Figure 1. General scheme of DEC systems

The energy inputs to a DEC system consist of the regeneration heat, the cooling load and the electricity for the auxiliaries. The cooling unit may be either an evaporative cooler or a VCC. In order to minimize the

electricity consumption, it is interesting to consider evaporative cooling units, which utilize water as working fluid. The present paper focuses on the modeling of a regenerative indirect evaporative cooler, the so-called Dew Point Cooler (DPC). The same component was studied by Janssen and Uges (2010), who built a prototype and tested it. They used the experimental results to validate their own DPC model, allowing an optimization of its dimensions based on a tradeoff between cooling performance and pressure drops. Their results allowed *StatiqCooling* to manufacture different DPC sizes. The model introduced in this paper is meant to be used for a complete DEC system analysis, as presented in Bellemo (2011). Goldsworthy and White (2011) studied an analogous DEC system design. In comparison with indirect evaporative coolers the DPC does not require an external secondary airstream because of its regenerative arrangement, i.e. lower temperatures than the wet bulb temperature of the incoming airstream can be reached, as also discussed by Riangvilaikul and Kumar (2010). In comparison with direct evaporative coolers the process airstream is cooled and kept at the same humidity ratio: from a system point of view less dehumidification is required, and precooling by heat recovery units may not be needed.

The investigated DPC cools the primary airstream at constant humidity ratio. The primary airstream flows into primary channels; afterwards is split into two airstreams: the supply airstream and the secondary airstream. The splitting is made possible by a system of dampers. The secondary airstream is recirculated back in the DPC, into secondary channels, where the evaporative cooling process takes place. Water is sprayed on the top, wetting thin hygroscopic foils that are spot-welded on the outside of the plates constituting the primary channels. The plates are made of polypropylene. The external and internal structures of the DPC are shown in Fig. 2. The internal dimensions are not stated by the manufacturer; therefore they are set to match the pressure drops declared by the manufacturer.

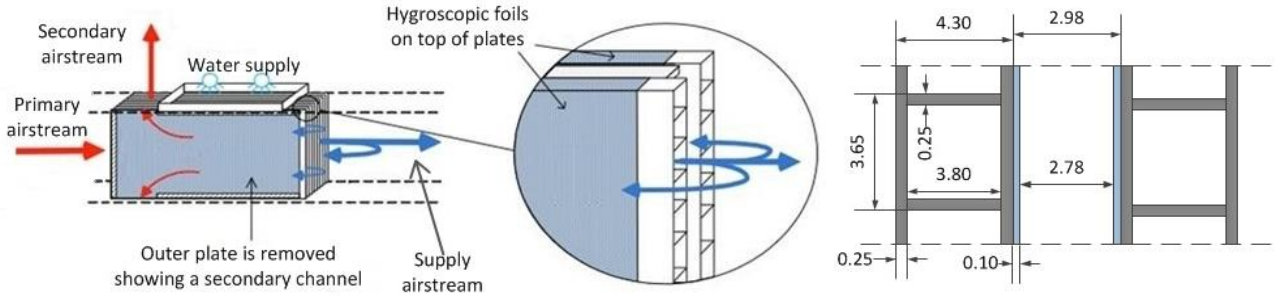

Figure 2. DPC structure (external side view on the left as shown by Janssen and Uges (2010), internal front view on the right - dimensions in [mm])

Theoretically this arrangement allows the primary airflow to be cooled from its inlet conditions to the corresponding dew point, i.e. the minimum temperature that can be reached.

The water sprayed on the DPC may require filtration and softening processes to avoid internal deposits of lime, hence poorer performance of the hygroscopic foils.

2. MODEL FORMULATION

The mathematical model of the DPC is based on first principles, implemented and solved in *Engineering Equation Solver* (EES).

2.1 DPC model

The DPC is modeled to simulate the cooling of dehumidified air in a DEC system, enabling realistic estimations of the supply conditions and the corresponding required amounts of water and electricity. Moreover, the model is a tool to estimate and optimize the DPC performance.

The model is based on the following assumptions:

- The cooler is not exchanging heat with the surroundings.
- The air flows are evenly distributed among the channels.

- Heat conduction in the flow direction is neglected.
- Heat transfer in the vertical direction is neglected.
- The water distribution on top of the cooler is homogeneous.
- The vertical water distribution is homogeneous.
- The hygroscopic foils adhere to the plates perfectly.
- The hygroscopic foils are modeled as layers of water with negligible thermal resistance.

Under these assumptions, the smallest constitutive unit of the DPC is modeled, including half of a primary channel, half of a secondary channel, the hygroscopic layer and plate in between, along the whole DPC length. This unit is further discretized into smaller control volumes (CVs) along the DPC length. The modeled geometry is shown in Fig. 3.

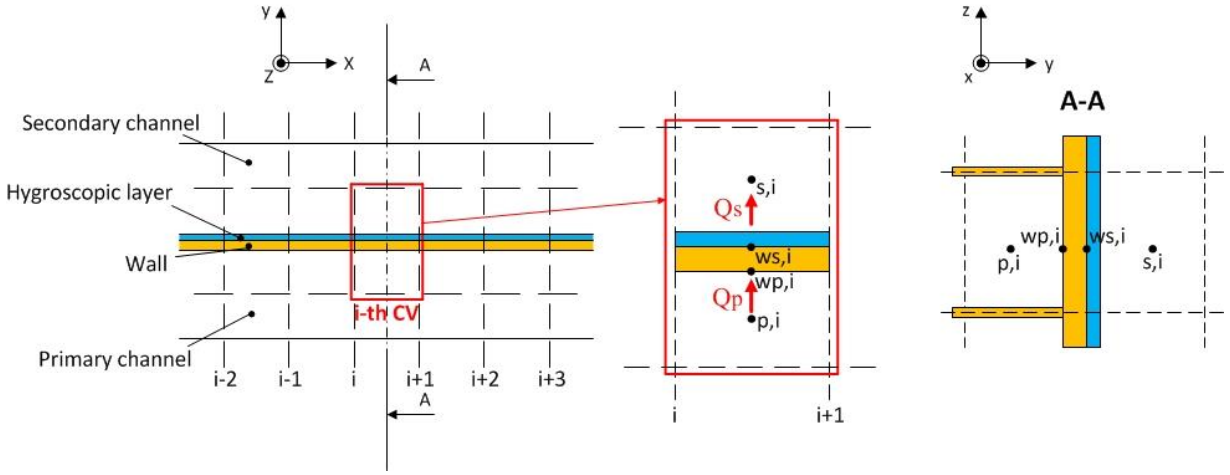

Figure 3. Discretization of the geometry

The governing equations for heat and mass transfer are discretized according to Fig. 3. The mass balances ensure conservation of the dry air mass flows in both sides and water vapor in the primary side, while in the secondary side also the evaporating water flow is accounted in the balance.

In the primary side, the energy balance for the generic i[th] control volume is expressed as:

$$\dot{m}_{a,p} \cdot \left(I_{p,i+1} - I_{p,i}\right) - \dot{Q}_{p,i} = 0 \quad (1)$$

Where $\dot{Q}_{p,i}$ is the sensible heat flux in [W] leaving the primary airstream, $\dot{m}_{a,p}$ is the primary mass flow of dry air in [kg_a/s] and $I_{p,i}$ is the specific enthalpy in [J/kg_a].

The sensible heat flux is determined by:

$$\dot{Q}_{p,i} = \bar{h}_{p,i} \cdot A_{p,i} \cdot \left(\bar{T}_{p,i} - \bar{T}_{wp,i}\right) \quad (2)$$

Where $\bar{T}_{p,i}$ and $\bar{T}_{wp,i}$ are the primary airstream and wall temperatures in [°C], respectively. $\bar{h}_{p,i}$ is the local heat transfer coefficient in [W/m^{2}K]. The bars indicate quantities referring to cell centered positions.

$\bar{h}_{p,i}$ is computed using the EES built-in correlation for duct flow. This correlation incorporates laminar, transition and turbulent flow; however, only laminar flow occurs for the whole range of conditions in this study. The upper and lower walls of the primary ducts are considered as fins, thus the primary side area $A_{p,i}$ [m^2] is corrected using the fin efficiency.

The thermal resistance of the wall $R_{w,i}$ in [K/W] is taken into account to compute the wall temperature in the secondary side $\bar{T}_{ws,i}$:

$$\dot{Q}_{p,i} = \frac{\bar{T}_{wp,i} - \bar{T}_{ws,i}}{R_{w,i}} \quad (3)$$

The hygroscopic foil is modeled as a layer of water. During steady state operation, some of this water evaporates and the corresponding water vapor $\dot{m}_{e,i}$ [kg/s] flows into the secondary airstream. The water content of the foils is maintained by the flow through the nozzles. In addition, the thermal resistance of the layer is considered negligible. The energy balance in the layer is:

$$\dot{Q}_{p,i} = \dot{Q}_{s,i} + \dot{m}_{e,i} \cdot C_{p,water} \cdot \left(\bar{T}_{ws,i} - T_{water,i}\right) = \dot{Q}_{s,i} + \dot{Q}_{water} \quad (4)$$

(5)

The second term on the right hand side accounts for bringing the added water in equilibrium with the adjacent wall. The remaining heat flux $\dot{Q}_{s,i}$ flows to the secondary side.

In the secondary side, the energy balance is expressed as:

$$\dot{m}_{a,s} \cdot \left(I_{s,i+1} - I_{s,i}\right) + \dot{Q}_{s,i} = 0 \quad (6)$$

$\dot{m}_{a,s}$ is proportional to $\dot{m}_{a,p}$ by defining the recirculation fraction f_{rec} as the ratio between the secondary and primary air volume flow rates.

$\dot{Q}_{s,i}$ is computed as the sum of the sensible and latent heat flows:

$$\dot{Q}_{s,i} = \dot{Q}_{s,sens,i} + \dot{Q}_{s,lat,i} \quad (7)$$

$$\dot{Q}_{s,sens,i} = \bar{h}_{s,i} \cdot A_{s,i} \cdot (\bar{T}_{ws,i} - \bar{T}_{s,i}) \quad (8)$$

$$\dot{Q}_{s,lat,i} = r \cdot \dot{m}_{e,i} = r \cdot \bar{\sigma}_i \cdot A_{s,i} \cdot \left(\omega_{ws,i} - \omega_{s,i}\right) \quad (9)$$

The local heat transfer coefficient $\bar{h}_{s,i}$ is again computed using the EES built-in correlation for duct flow. The heat and mass transfer analogy is used to compute the local diffusion mass flux $\bar{\sigma}_i$ in [kg/m^{2}s] as presented in Mills (2001): the local Sherwood number is calculated by replacing the local Prandtl number with the local Schmidt number in the EES built-in correlation providing the local Nusselt number.

Due to the simplifications of the model the mass transfer capacity of the secondary side may be sufficient to reach over-saturated conditions. However, this is not a realistic operating condition. In this it the secondary airstream is limited to saturated conditions and the amount of evaporating water is adjusted accordingly.

Along the DPC entrance, an area effectiveness coefficient η_s of 0.1 is applied to half of the length where water is not sprayed on top. Such a low value is motivated by the fact that the airstreams have a cross flow arrangement, the secondary airstream splits exiting both at the top and bottom of the cooler, and the absence of the spraying box on top leads to non-optimal wetting of the hygroscopic foils.

Pressure losses are estimated for both the primary and secondary airstreams, considering three contributions: pressure drop due to initial acceleration, pressure drop due to internal friction, and pressure gain due to final deceleration of the airstream. These terms are defined as presented by Mills (1999). The friction factors for laminar flows are inversely proportional to the Reynolds number.

2.2 DPC geometry

The DPC characteristics are taken from manufacturer specifications. The biggest available DPC size is considered. However, the mathematical formulation and the computational strategy used for the model are independent of the component size. The considered DPC characteristics are reported in Table 1. The internal geometry is reported in Fig. 2.

Table 1. Characteristics of the modeled DPC

Length [m]	1.38
Height [m]	1.50
Number of plates	70
Nominal primary volumetric airflow rate [m^3/h]	4200
Maximum primary volumetric airflow rate [m^3/h]	5600

3. RESULTS

3.1 DPC model analysis

Fig. 4 illustrates the results of the model. State 1 is the inlet air condition. This is cooled to state 2 by the secondary side. Secondary air inlet, state 3, is recirculated air from the primary side, which is humidified and heated to reach state 4. The points on the curves indicate the state change of the primary air (1-2) and secondary air (3-4) along the control volume centers of the DPC. The reference inlet conditions for the primary airstream and water are reported in Table 2, reflecting possible working conditions in a DEC system: the primary airstream is dehumidified and heated in the desiccant dehumidifier, and precooled in an air to air heat recovery unit as explained in Bellemo (2011). The manufacturer suggests to set f_{rec}=30%.

Table 2. Reference conditions for the analysis of the DPC model

T_1 [°C]	ϕ_1 [%]	ω_1 [g_v/kg_a]	T_{DP1} [°C]	$\dot{V}_1$ [m^3/h]	f_{rec} [%]	T_5 [°C]
35	25	8.8	12	4200	30	15

Where $T_{DP1}$is the dew point of the primary airstream and T_5 is the sprayed water temperature.

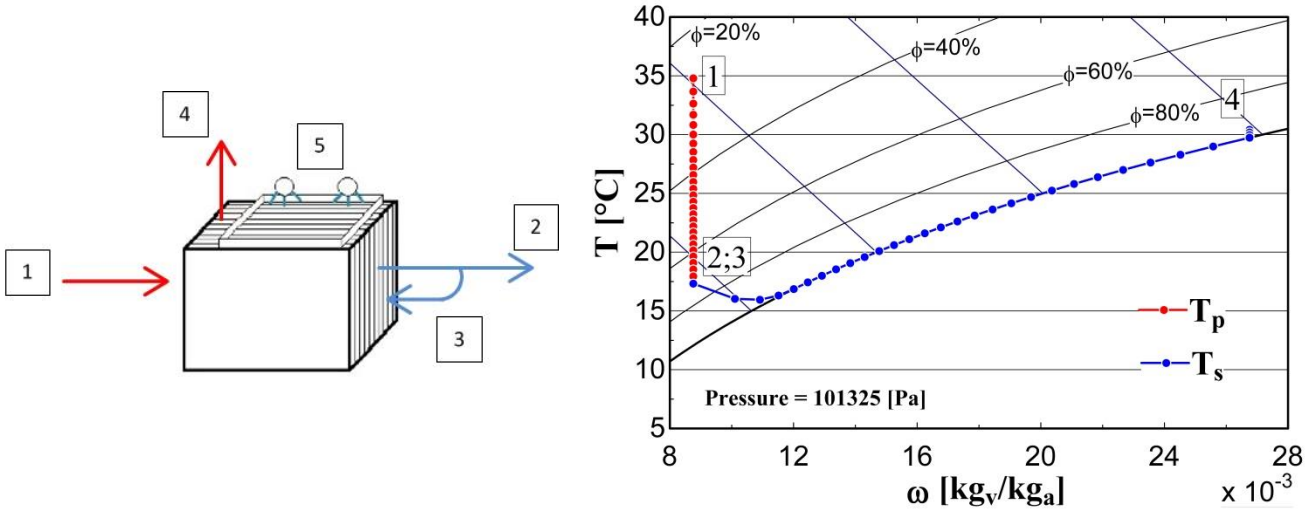

Figure 4. DPC psychrometrics (1-2 Primary flow, 3-4 Secondary flow)

The primary airstream is cooled maintaining a constant humidity ratio, while the secondary airstream is both adiabatically humidified by the evaporative process and heated. The resulting primary outlet temperature T_2 is 17.3 [°C], while the secondary outlet temperature and relative humidity are 30.4 [°C] and 96%. The pressure losses are 202 [Pa] and 128 [Pa] for the primary and secondary airstreams respectively.

The effectiveness of the DPC is defined as below, as the inlet air cannot reach a lower temperature than the inlet temperature of the secondary side, which in an ideal DPC would be the dew point temperature of the primary air:

$$\varepsilon_{DPC} = \frac{T_1 - T_2}{T_1 - T_{DP1}} \tag{10}$$

In this case, the computed DPC effectiveness is 77%.

Fig. 5a shows the airstreams and walls temperature profiles along the DPC length. Fig. 5b shows the heat flows in the secondary airstream and water layer at the center of single CVs along the DPC length.

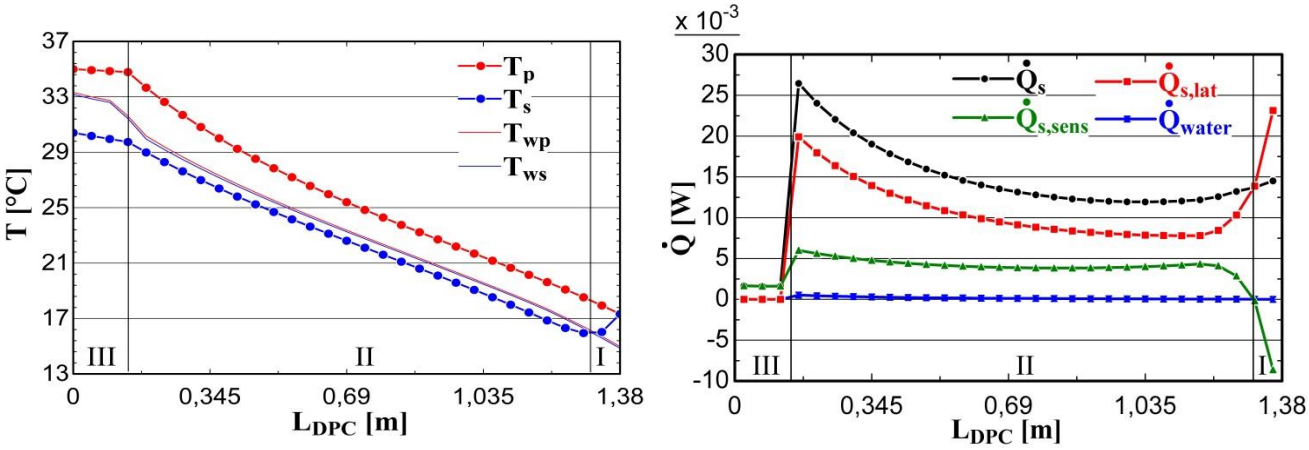

a) Temperature b) Heat transfer

Figure 5. Internal temperature and heat transfer profiles

It is observed that $\dot{Q}'''_{water}$ has a negligible contribution in the overall energy balance. Considering the secondary airstream, three different zones are identified:

I) The secondary airstream enters the DPC at the primary side outlet conditions. The wall is cooled by the evaporation process, which is initially high as indicated by the latent heat flow. Mass transfer potential in this zone is high, increasing as much as the inlet conditions of the secondary airstream are far from saturation. The resulting sensible heat flow is negative: heat goes from the secondary airstream to the water layer.

II) The secondary airstream becomes colder than the adjacent wall: sensible heat flows from the wall to the airstream. Latent heat flow decreases with the secondary airstream approaching saturation. Then sensible and latent flows increase gradually: the temperature profile of the secondary airstream is almost linear.

III) Before the secondary airstream leaves the DPC, it encounters a zone where the potential for heat and mass transfer is strongly reduced. The reduced heat flows induce a flattening of the temperature profiles.

3.2 Sensitivity analysis

The primary airstream inlet conditions are varied individually to analyze the DPC performance, estimated by the DPC effectiveness, the DPC cooling capacity ($\dot{Q}_{DPC}$), the DPC net cooling capacity ($\dot{Q}_{DPC,net}$), and the primary airstream outlet temperature. $\dot{Q}_{DPC}$ is the heat flow rate from the primary to the secondary airstream, while $\dot{Q}_{DPC,net}$ is the supplied cooling flow rate:

$$\dot{Q}_{DPC} = \dot{m}_{a,p} \cdot (I_1 - I_2) = \dot{m}_{a,p} \cdot \overline{C_p} \cdot (T_1 - T_2) \tag{11}$$

$$\dot{Q}_{DPC,net} = (\dot{m}_{a,p} - \dot{m}_{a,s}) \cdot (I_1 - I_2) = \dot{m}_{a,p} \cdot \left(1 - f_{rec} \cdot \frac{\rho_3}{\rho_1}\right) \cdot \overline{C_p} \cdot (T_1 - T_2) \tag{12}$$

An analysis of the DPC performance on the primary inlet thermo-hygrometric conditions is shown in Fig. 6.

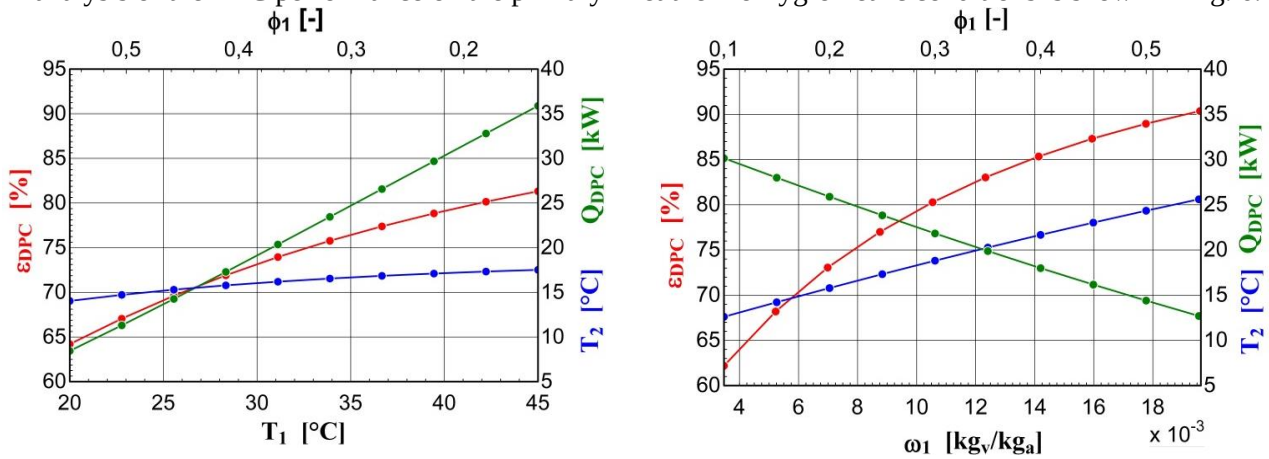

a) Constant inlet humidity ratio (ω_1=8 [g_v/kg_a]) b) Constant inlet temperature (T_1=35 [°C])

Figure 6. Analysis on primary inlet thermo-hygrometric conditions ($\dot{V}_1$=4200 [m^3/h], f_{rec}=0.3)

It is demonstrated that ω_1 has the biggest influence on T_2: in Fig. 6a ω_1 is kept constant, leading to a much smaller change in T_2 in comparison to Fig. 6b, where T_2 increases linearly at a rate of approximately 0.8[°C/(g_v/kg_a)]. In Fig. 6a ε_{DPC} varies according to T_2, since $T_{dp,1}$ is kept constant. $\dot{Q}_{DPC}$ strongly increases because T_2 only varies to a small extent. In Fig. 6b ε_{DPC} varies differently from T_2: both $T_2$and $T_{dp,1}$ vary, with $T_{dp,1}$ following the saturation curve on the Mollier diagram. In this case $\dot{Q}_{DPC}$ decreases, since the difference between T_1 and T_2 decreases and is approaching saturated conditions.

The effect of varying primary inlet flow rates and recirculation fractions is shown in Fig. 7.

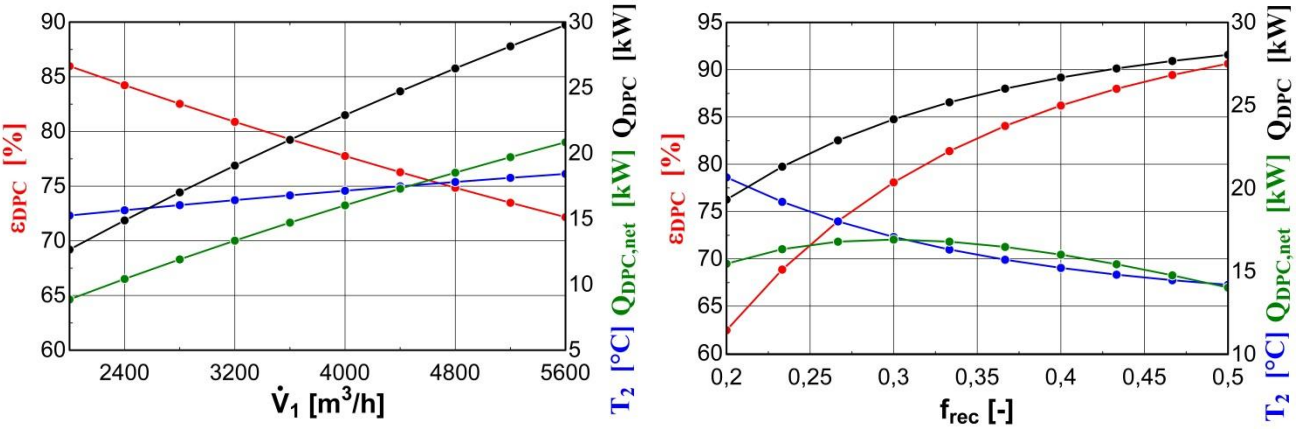

a) Constant recirculation fraction (f_{rec}=30%) b) Constant primary airflow rate ($\dot{V}_1$=4200 [m^3/h])

Figure 7. Analysis on primary and secondary flow rates (T_1=35 [°C], Φ_1=25%)

Fig. 7a shows that T_2 is directly proportional to $\dot{V}_1$, but scarcely affected. Therefore, ε_{DPC} decreases for increasing $\dot{V}_1$, while $\dot{Q}_{DPC}$ increases. Fig. 7b shows that both ε_{DPC} and $\dot{Q}_{DPC}$ increase for increasing f_{rec}, with a corresponding decrease of T_2. From these observations it could be argued that higher f_{rec} leads to a better DPC performance. However, $\dot{Q}_{DPC,net}$ reaches a maximum for f_{rec} around 0.3. This result indicates that the supplier recommendation and the model are in accordance.

3.2 DPC model validation

The DPC model presented above was based on parameters from literature and estimates. It was found to show better performance than presented by the manufacturer. To better account for the non-ideal characteristics, the model has been validated and tuned by using manufacturer data. Several steady state operating conditions are considered by varying the input parameters. Some of these states are reported in Table 3. The corresponding performance data from the DPC model, manufacturer and the tuned DPC model are presented in Table 4 and Table 5**.**

Table 3. Steady states for performance comparison

Steady state	$\dot{V}_{p,in}[m^3/h]$	f_{rec}[%]	$T_{p,in}$ [°C]	$\Phi_{p,in}$[%]
1 Reference	4200	30	35	25
2 High flow	5600	30	35	25
3 Low flow	3000	30	35	25
4 Hot inlet	4200	30	45	15
5 Humid inlet	4200	30	35	40
6 High recirculation	4200	50	35	25

Table 4. Heat and mass transfer performance comparison

	Manufacturer data			**DPC model (η_s=1)**			**Tuned DPC model (η_s=0.55)**		
State	ε_{DPC} [%]	$\dot{Q}_{DPC}$ [kW]	$\dot{m}_e$ [kg/h]	ε_{DPC} [%]	$\dot{Q}_{DPC}$ [kW]	$\dot{m}_e$ [kg/h]	ε_{DPC} [%]	$\dot{Q}_{DPC}$ [kW]	$\dot{m}_e$ [kg/h]
1	65	20.9	23.7	78	24.2	28.4	66	20.4	25.3
2	58	25.1	29.7	74	30.4	36.3	60	24.6	31.7
3	72	16.4	18.1	82	18.2	21.0	72	16.0	19.2
4	71	30.9	35.6	83	35.4	42.4	71	30.2	38.0
5	73	16.0	18.4	87	18.3	21.6	74	15.5	19.5
6	76	24.2	26.0	91	28.0	30.4	76	23.6	28.0

As explained the initial model shows the best performance. The tuned DPC model is characterized by an area effectiveness coefficient which is kept constant at 0.55, but maintaining a value of 0.1 at the DPC entrance. The effectiveness, cooling capacity and water flow rate estimated by the tuned model deviate from the manufacturer data within 4%, 3% and 8% respectively.

Table 5. Pressure drops comparison

	Manufacturer data		**DPC model**	
State	$\Delta P_{primary}$ [Pa]	$\Delta P_{secondary}$ [Pa]	$\Delta P_{primary}$ [Pa]	$\Delta P_{secondary}$ [Pa]
1	202	131	203	128
2	269	175	273	176
3	144	94	144	89
4	208	136	205	128
5	202	131	204	129
6	202	219	202	221

The computed pressure drops deviate from the manufacturer data within 2% and 6% respectively.

4. DISCUSSION

The area effectiveness coefficient used in the tuned model is 0.55, meaning that only half of a real DPC works at the conditions used to build the model, while the rest does not contribute, according to manufacturer data. In practice the area effectiveness coefficient varies locally within a wide range. An important cause of performance loss is the inhomogeneous water distribution in the DPC, which results in unsaturated water vapor conditions at the surface of the hygroscopic foils. Water distribution problems may be caused by clogging and increased absorptive resistance in the hygroscopic foils. Another important cause may be the air distribution in the DPC, influenced by internal pressure losses, the geometry of the connecting ducts to the system, and the direction change imposed to the outgoing secondary airstream. Supposing that the connecting ducts have gradual contraction/divergence such to not affect the airflow distribution, the internal pressure losses may differ because of partial bending of the channels since the DPC structure is made of polypropylene. Moreover, the hygroscopic foils are spot-welded on the DPC structure, with the possibility of an imperfect contact between the layers, increasing the thermal resistance. All these effects are not covered by the initial model. The difference in performance between the initial model and the data is proposed to be caused by these effects. Measurements on a real DPC and CFD analysis are suggested as future work to improve the DPC performance.

5. CONCLUSION

The built model is based on first principles using a 1D finite volume scheme to determine the steady state working conditions of the DPC. The model can determine both maximum and realistic DPC performance. It is found that realistic performances correspond to an area effectiveness coefficient of 0.55. Additionally, the model enables calculations of the required amounts of water and electricity. The relative simplicity of the

model makes it suitable to be used into complete steady state system analyses. The sensitivity analysis reveals that the DPC net cooling capacity is maximized for a recirculation fraction around 30%. Moreover, it is shown that the primary inlet humidity ratio has the strongest influence on the supply temperature. This result is important from a system point of view: the supply humidity ratio may be set lower than what required by energy and mass balances in the conditioned space to supply colder air, or, maintaining the same supply temperature, reduce the required number of DPCs. The supply temperature also decreases with decreasing primary airstream inlet temperature and flow rate, but to a lower extent. The results show that the DPC effectiveness alone is not sufficient to evaluate the DPC performance: it may increase either for increasing supply temperatures or for decreasing temperature differences between inlet and supply conditions.

REFERENCES

Bellemo L., 2011. New desiccant cooling system using the regenerative indirect evaporative process. MSc thesis. Technical University of Denmark, Department of Mechanical Engineering, Section of Thermal System.

Daou K., Wang R., Xia Z., 2006. Desiccant cooling air conditioning: a review. Renewable and Sustainable Energy Reviews, vol. 10, no. 2, pp. 55–77.

Goldsworthy M., White S., 2011. Optimisation of a desiccant cooling system design with indirect evaporative cooler. International Journal of Refrigeration, vol. 34, issue 1, pp. 148–158.

Janssen M., Uges P., 2010. Parameters affecting the performance of a dewpoint cooler consisting of a counter flow heat exchanger using water as refrigerant. 9th IIR Gustav Lorentzen Conference, Sydney.

Mills A., 1999. Heat Transfer, Prentice Hall, pp. 811-817.

Mills A., 2001. Mass Transfer, Prentice Hall.

Riangvilaikul B., Kumar S., 2010. Numerical study of a novel dew point evaporative cooling system. Energy and Buildings, vol. 42, issue 11, pp. 2241-2250.

StatiqCooling. Available at: <http://www.statiqcooling.nl/> [accessed 6.4.2013].